Perspectives for Intersubband Polariton Lasers

Raffaele Colombelli* and Jean-Michel Manceau

Institut d'Electronique Fondamentale, Université Paris Sud, UMR8622 CNRS, 91405 Orsay, France

(Received 3 October 2014; revised manuscript received 23 January 2015; published 23 March 2015)

Cavity polaritons are mixed states, partially microcavity photon and partially material excitation, which behave as bosons up to a critical density. In the case of excitonic polaritons, the critical parameter is the Mott density, which cannot be tailored, in a given material system. Interestingly, in the case of intersubband polaritons, such critical density can be engineered to a large extent via the doping. We show that this observation has crucial implications for intersubband polariton lasers, and we make a strong case in favor of their development.

DOI: 10.1103/PhysRevX.5.011031 Subject Areas: Optoelectronics, Semiconductor Physics

We are accustomed to optoelectronic devices operating in the weak-coupling regime between light and matter. Conventional lasers, for instance, operate in this regime and rely on population inversion to achieve optical gain. Recent years have seen a surge of interest for quantum systems operating in the strong-coupling regime instead, i.e., when the coupling strength for the light-matter interaction is so strong that perturbation theory no longer suits the description of the system. The new eigenmodes are a superposition of states—partially light, partially material excitation—called cavity polaritons.

In the realm of semiconductors, exciton polaritons are the most widely studied. Originally reported in 1992 [1], it was soon clear that their extremely light mass—together with the bosonic character inherited from the excitonic component—could lead to Bose-Einstein condensates at relatively high temperatures. In a two-dimensional system, the condition for quantum degeneracy is [2]

$$\frac{n}{k_B T} \geq \frac{2m^*}{h^2}, \tag{1}$$

where n is the polariton 2D density, k_B is the Boltzmann constant, T is the temperature, h is the Planck constant, and m^* is the polariton effective mass. The m^* is dominated by the photon, and it results in a polariton mass orders of magnitude lighter than the exciton one. Formula (1) implies that polaritonic condensates can exist at much higher temperatures (few hundreds of Kelvin) than excitonic ones (mK) [3]. The successful observation of polaritonic condensates in several material systems (GaAs, CdTe, GaN, ZnO) spawned a new, exciting research field. In particular, the quantum properties of the condensates are the subject of intense investigation. A good review of the current state of the art can be found in Ref. [4].

In this context, a different type of "laser" was proposed in 1996 [5], which does not rely on population inversion but on bosonic final-state stimulation. In a bosonic system, the probability of transition toward a final state is proportional to the population of said state [4]. Polariton lasing happens when the scattering time toward the ground state—typically at $k = 0$—is shorter than the lifetime of the final state. The population then builds up abruptly, and the output power is

$$P_{\text{out}} = \frac{\hbar\omega N}{\tau_{\text{rad}}} S, \tag{2}$$

where ω is the photon frequency, N is the polariton 2D density in the final state, τ_{rad} is the radiative lifetime of the final state, and S is the device surface. The effect has been demonstrated in several exciton-polariton systems under optical pumping [6–8]. More recently, exciton-polariton lasing under electrical pumping at room temperature was reported at $\lambda \sim 365$ nm in the GaN material system [9]. These beautiful and elegant demonstrations exploit the fascinating phenomenon that is Bose-Einstein condensation. Their applicative potential is still untapped, however, because the output power is in general very low, although the recent demonstration in Ref. [9] provides perspectives for low-power-consumption devices. For certain materials, it is also difficult to operate the devices at room temperature, while for others (GaN, ZnO), it is instead possible [10].

Note that in formula (1), the polariton density cannot be chosen at will but must comply with the upper limit set by the Mott transition density (n_{Mott}). Above n_{Mott}, excitons—and polaritons, too—cannot be considered bosons anymore since the interparticle distance becomes comparable to the radius of the exciton. For instance, n_{Mott} in GaAs, CdTe, and GaN quantum wells (QWs) are, respectively, 2×10^{11}, 1×10^{12}, and 4×10^{12} cm^{-2}. Let us assume that a polariton laser operates safely in the "bosonic" regime up to 20% of

*raffaele.colombelli@u-psud.fr

the Mott density. The loss of bosonicity for polariton densities above this value puts an intrinsic upper limit to the available output power, via formula (2), and also to the maximum operating temperature, via formula (1).

Recently, polaritons have been explored in a different system, where the material excitation is an intersubband (ISB) transition (or, to be more rigorous, an ISB plasmon) in a semiconductor QW. They are called intersubband polaritons [11]. ISB transitions constitute the backbone principle behind quantum cascade (QC) lasers. Their design flexibility (the ISB transition energy can be tailored over a broad wavelength range by changing the layer thickness) has been the key ingredient that makes QC lasers effective coherent mid-IR semiconductor sources, and also promising THz sources (albeit, the problem of the maximum operating temperature is still a major issue for operation in the THz range of the electromagnetic spectrum [12]). Transferring such flexibility into the realm of polaritons has been one of the motivations behind the development of ISB polaritonics.

ISB polaritons were observed for the first time in the mid-IR range of the electromagnetic spectrum [11]. It was soon highlighted that ISB optoelectronic devices operating in strong coupling had potential for applications and fundamental research [13]. Since then, several developments have taken place: ISB polariton light-emitting devices (LED) [14] almost simultaneously with exciton-polariton LEDs at near-IR (NIR) wavelengths [15–17], detectors [18], emitters [19,20], and all-optical ultrafast control [21,22]. Recent studies have targeted the THz range, where new challenges are appearing, such as the so-called ultra-strong-coupling regime [23–26], and proposals to achieve THz emission exploiting upper-to-lower polariton transitions using asymmetric QWs [27].

In the context of final-state stimulated scattering, the bosonic character of ISB plasmons—and hence of ISB polaritons—is of crucial importance. They are composite bosons, under certain limits. As discussed in Refs. [28,29], if $b^{+}_{\mathbf{q}}$ is the creation operator of the bright ISB excitation with wave vector $\mathbf{q}$, the commutation operator taken on a state $|\phi\rangle$ with N_{exc} ISB excitations is

$$\langle\varphi|b_{\mathbf{q}'}, b^{+}_{\mathbf{q}}|\varphi\rangle = \delta_{\mathbf{q}',\mathbf{q}} + o\left(\frac{N_{\mathrm{exc}}}{n_{\mathrm{QW}}N_{\mathrm{el}}}\right), \tag{3}$$

where n_{QW} is the QW number and N_{el} is the total of the number of electrons in the QW. Formula (3) states that the commutator is bosonic, provided that a limited number of excitations is present, i.e., that $N_{\mathrm{exc}} \ll n_{\mathrm{QW}}N_{\mathrm{el}}$.

This observation suggests that a new degree of freedom is present: In ISB polariton systems, the upper density limit for bosonic operation is no more rigidly fixed—as is the case of the Mott density for excitons—but it can be engineered by design to a large extent with the electronic doping. The maximum temperature at which an ISB polariton condensate can be sustained [formula (1)] and the maximum output power of an ISB polariton laser [formula (2)] can therefore be maximized in highly doped systems.

Motivated by the aforementioned considerations, we develop a perspective based on a semiquantitative analysis of realistic device architectures. We show that intersubband polariton lasers exhibit design flexibility and a vast potential for applications, and we make a strong case toward their development. Finally, a roadmap to achieve this goal is proposed.

We analyze three model situations: the THz ($\lambda = 100\ \mu$m) in the GaAs/AlGaAs system, the mid-IR ($\lambda = 10\ \mu$m) in the InGaAs/AlInAs system, and the near-IR ($\lambda = 1.55\ \mu$m) in the GaN/AlN system. A schematic of the three situations is depicted in Fig. 1, with Table I summarizing the important material and resonator parameters. The maximum doping (n_{max}) is the sheet electronic doping level at which the second subband of the QW starts to be filled with electrons: It naturally increases with the transition frequency. τ_{ISB} is the total lifetime of the ISB transition: It is dominated by the intrasubband dephasing time, which stems from electron-electron and electron-impurity scattering. Note that τ_{ISB} is much shorter than the LO-phonon emission time, of the order of a few ps, which is instead relevant for quantum cascade laser physics. $\tau_{\mathrm{ISB\text{-}rad}}$ is the radiative lifetime, and it is calculated with the standard Fermi golden rule [30] and correctly scales with the third power of the emission frequency. Note that a major difference with respect to exciton-polariton systems is that the lifetime is dominated by nonradiative processes.

The microcavity resonator is the second important ingredient. We select optical resonators that offer an energy minimum at $k_{\parallel} = 0$ with a positive, parabolic dispersion. Essentially, we aim to mimic the polaritonic dispersion of exciton-polariton systems based on Fabry-Perot cavities (as schematically depicted in Fig. 2), which has been the

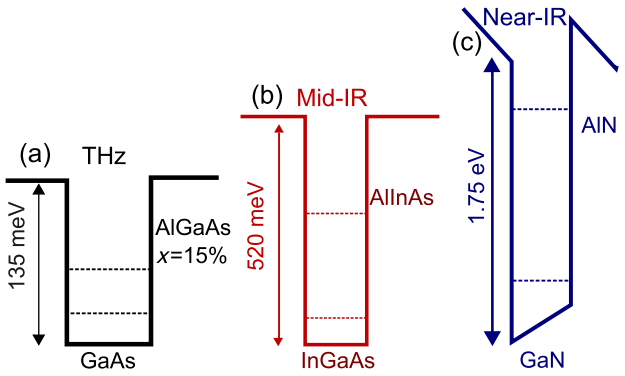

FIG. 1. Conduction-band energy profile of semiconductor QWs for the three different spectral regions studied in this work. (a) GaAs/$Al_{0.15}GaAs_{0.85}$ with a band offset of 135 meV for the THz range, (b) InGaAs/AlInAs with a band offset of 520 meV for the mid-IR range, and (c) Gan/AlN with a band offset of 1.75 eV in the near-IR range.

TABLE I. Summary of the important material and cavity parameters for the three material systems considered in this work. τ_{ISB} has been estimated, taking as 3% the best FWHM achievable in the mid-IR with modulation-doped structures [31] and 5% in the THz. The respective cavity geometries used for each range are represented on top. PhC stands for photonic crystal.

	THz	Mid-IR	Near-IR
λ	100 μm	10 μm	1.5 μm
QW width	30 nm	10 nm	1 nm
Maximum doping	4.5×10^{11} cm^{-2}	2×10^{12} cm^{-2}	5×10^{12} cm^{-2}
τ_{ISB}	1 ps	0.2 ps	0.08 ps
$\tau_{ISB\text{-}rad}$	90 μs	90 ns	0.3 ns
$Q_{cav\text{-}rad}$	100 (metallic PhC)	100 (metallic PhC)	10 000 (membrane PhC)
$\tau_{cav\text{-}rad}$	5 ps	0.5 ps	8 ps
$Q_{cav\text{-}tot}$	25	20	5000
$\tau_{cav\text{-}tot}$	1.3 ps	0.1 ps	4 ps

enabling tool behind the demonstration of exciton-polariton lasers [2,5]. The dispersion is crucial, as it enables polariton-polariton or polariton-phonon scattering processes—as depicted in Fig. 2—on which a polaritonic laser or amplifier relies. In the context of ISB polaritons, it is more effective at this time to rely on phonon-polariton scattering [32], as originally discussed in Ref. [28], since little is known yet about polariton-polariton processes [29].

We have recently shown in Refs. [33,34] that properly patterned metal-insulator-metal (MIM) resonators satisfy the aforementioned requirements in the THz and in the mid-IR ranges of the electromagnetic spectrum. They

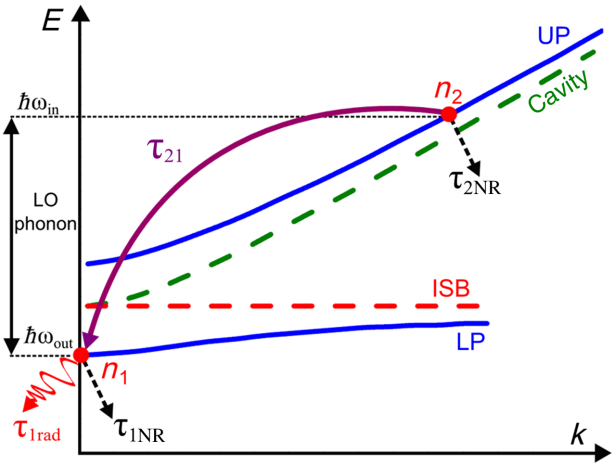

FIG. 2. Typical dispersion diagram of intersubband polaritons in a MIM cavity. The various loss channels are represented as well as the scattering mechanism based on the longitudinal optical phonon, which is relevant for the operation of a bosonic laser. The solid lines represent the two polariton eigenmodes, and the dashed lines are the bare cavity and ISB eigenstates.

are sketched in the upper section of Table I. Such microcavities are extremely practical: They can be optically probed in reflectivity and optically pumped at variable incidence angles, and electrical injection can be easily implemented. The experimentally measured total quality factor $Q_{cav\text{-}tot}$ (lower limit) is approximately 20, and the radiative one $Q_{cav\text{-}rad}$ is approximately 100. The lifetimes are readily obtained using the relationship $Q = \omega\tau$.

As per the near-IR case, ISB transitions in GaN at short wavelengths have been experimentally observed for a few years [35–38], and it has been recently demonstrated that GaN suspended-membrane photonic crystal cavities can be implemented with Q_{tot} in the thousands [39,40]. We assume $Q_{cav\text{-}tot} = 5000$ and $Q_{cav\text{-}rad} = 1000$. To take advantage of these very high Q factors, however, the coupling to the cavity must be implemented with evanescent fiber couplers [41,42].

Using the lifetime values of Table I, we calculate the total and radiative lifetimes of the polaritonic states and the radiative efficiency of the polaritonic system as a function of the Hopfield coefficients. The eigenstates of the coupled system are a linear superposition of the uncoupled eigenstates $|\psi_{i,k}\rangle$ (with $|\psi_{1,k}\rangle$ the fundamental state and $|\psi_{2,k}\rangle$ the excited one) and $|n\rangle$ the state with n photons in the cavity:

$$|\mathrm{UP}\rangle = \alpha_{\mathrm{UP}}|\psi_{1,k}, 1\rangle + \beta_{\mathrm{UP}}|\psi_{2,k}, 0\rangle,$$
$$|\mathrm{LP}\rangle = \alpha_{\mathrm{LP}}|\psi_{1,k}, 1\rangle + \beta_{\mathrm{LP}}|\psi_{2,k}, 0\rangle. \quad (4)$$

The coefficients $\alpha_{LP,UP}$ and $\beta_{LP,UP}$ are the Hopfield coefficients [43]. They permit us to gauge the weight of the photonic and material components within the polariton

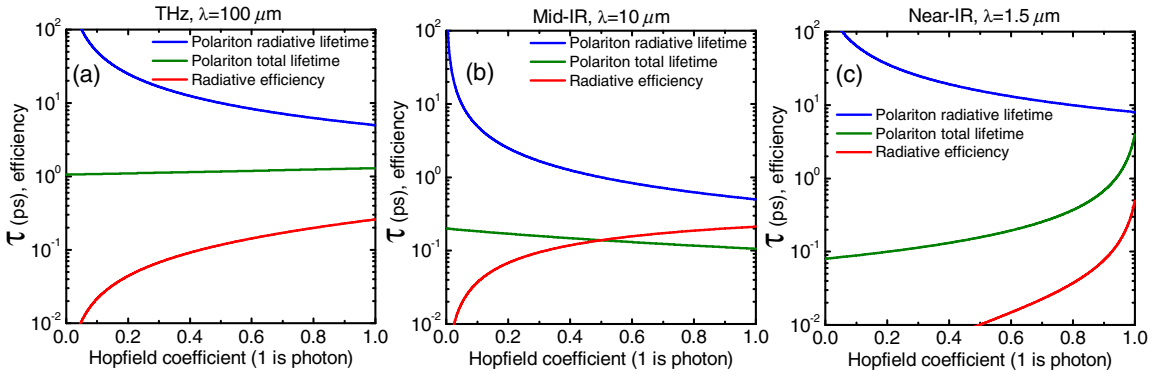

FIG. 3. Polariton radiative lifetime (solid blue lines), polariton total lifetime (solid green lines), and radiative efficiency (solid red lines) as a function of the lower polariton-state Hopfield coefficient. A value of 1 represents a full photonic component. (a) THz range, (b) mid-IR range, and (c) near-IR range.

branches. Their control is of crucial importance, since it permits us to tailor the polaritonic lifetimes, as follows:

$$\frac{1}{\tau_{\text{LP-rad,tot}}} = \frac{|\alpha_{\text{LP}}|^2}{\tau_{\text{cav-rad,tot}}} + \frac{1-|\alpha_{\text{LP}}|^2}{\tau_{\text{ISB-rad,tot}}}, \tag{5}$$

where τ_{LP} is the radiative or the total lifetime of the lower polariton state. Figure 3 reports the LP radiative and total lifetimes and the radiative efficiency (or internal quantum efficiency η_{QE}), as a function of $|\alpha_{\text{LP}}|^2$.

The first remark is that the internal quantum efficiency η_{QE} is approximately 10%, in the mid-IR and in the THz, for $|\alpha_{\text{LP}}|^2$ values above 0.4. This level of quantum efficiency represents an enhancement of approximately 3 orders of magnitude with respect to a bare ISB transition in the mid-IR and of 5 orders of magnitude in the THz. This prediction is in contrast with the experimental findings: A relatively wide range of mid-IR and THz electroluminescent polaritonic structures has been reported, and η_{QE} enhancements were never observed [19,20]. As per the near-IR case, ISB polaritons in the GaN/AlN system have not been demonstrated yet.

Intuitively, the enhancement argument is valid provided that the Rabi time is much faster than the polariton lifetime. A quick estimate using the formula $\Delta\tau \approx \hbar/\Delta E$, using approximate Rabi-splitting values of 30 meV in the mid-IR and 3 meV in the THz, yields Rabi times of 22 fs (220 fs) in the mid-IR (THz). Comparison with Fig. 3 points at the validity of the argument, since the estimated polariton lifetimes are longer. (Nevertheless, the larger the Rabi splitting, the better.) As a matter of fact, the observed lack of efficiency enhancement possibly stems from the pumping scheme, based on electronic injection. The electrical injection of ISB plasmons, as well of ISB polaritons, suffers from the same problem encountered in surface-plasmon generation [44]: Most of the energy is transferred to dark modes, which do not couple with the electromagnetic field [45,46]. However, this limitation is removed in the case of optical generation: The most promising course of action to investigate and demonstrate the η_{QE} enhancement in ISB polariton devices is to perform optical pumping experiments. In fact, the demonstration of η_{QE} enhancement constitutes a necessary first step toward the development of an ISB polariton laser: In the final section of the paper, we propose realistic structures operating in the mid-IR and relying on polariton-phonon scattering. Furthermore, Figs. 3(a) and 3(b) show that in the mid-IR and THz ranges, there is a LED-friendly region (with Hopfield coefficient above 0.5) where the calculated radiative efficiency is high (above 0.1) [47].

We now discuss the polariton lifetimes (radiative $\tau_{\text{pol-rad}}$ and total $\tau_{\text{pol-tot}}$). The blue curves in Fig. 3 correspond to the calculated radiative lifetime of the LP mode as a function of the Hopfield coefficients, for THz, mid-IR, and near-IR. In all cases, they lie in the ps or tens-of-ps range. A useful figure of merit to gauge the potential of a polaritonic LED or laser is the power per unit device surface P_S [P/S, according to formula (2)], which can be emitted by the device at a given polariton density. It is expressed in W/cm^2, and the results are reported in Fig. 4 for structures containing one single QW.

The black, red, and blue dashed lines correspond to the THz, mid-IR, and near-IR cases, respectively. The round dots mark the P_S at 20% of the maximum doping density as reported in Table I, which we consider the limit for safe bosonic operation of a polaritonic device. The green star marks the maximum P_S for a GaAs exciton-polariton LED operating at a shorter wavelength of 800 nm.

The first remark is that ISB polaritonic devices can all operate at higher polariton densities than exciton-polariton devices at approximately 800 nm. The important consequence, stemming from formula (1), is that ISB polariton lasers are, in principle, able to operate at room temperature. This observation is particularly significant in the THz range of the electromagnetic spectrum [12]. Note that here we have considered simple, square semiconductor quantum wells as a basis for discussion of possible condensation and

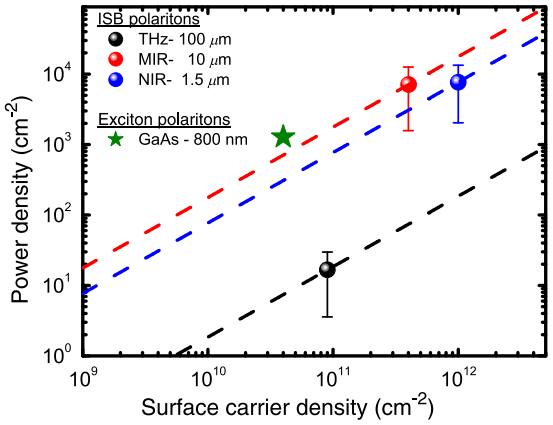

FIG. 4. Power density as a function of the surface carrier density of polaritons for the studied spectral regions. The green star marks the maximum power density for excitonic polaritons at 800 nm in the GaAs/AlGaAs inherently fixed by the Mott density.

"bosonic" lasing of ISB polaritons. This assumption is compatible with room-temperature operation for near-IR and mid-IR wavelengths. However, room-temperature operation with a square quantum well is problematic in the THz. The solution—omitted for simplicity—is to employ parabolic quantum wells [48,49], which can efficiently operate in the THz range up to room temperature [50]. Furthermore, thanks to the Kohn theorem [51], the effect of the depolarization shift can be neglected. As per ZnO- and GaN-based devices, they would deserve a separate discussion [10,52]. However, they operate at much shorter wavelengths $\lambda < 400$ nm; hence, we do not deal with them in this paper.

The second result is that the output powers achievable with ISB polariton LED and lasers are not marginal. For instance, with the data in Fig. 4, a THz polariton laser with the dimensions of a typical THz QC laser ($100 \times 1000\ \mu m^2$) would emit 15–20 mW, with only one QW and at room temperature. If we perform the same calculation for the mid-IR case, with a device size $10 \times 500\ \mu m^2$, we obtain 350 mW.

As a last remark, note that the maximum P_S for the exciton-polariton case (green star) lies a decade below the value for the mid-IR, although the photon energy is more than 10 times larger. It is due to the unavoidable limit represented by the Mott density, and it materializes the advantage provided by ISB transitions.

The question of whether or not an ISB polariton laser can be implemented depends on the total polariton lifetime, which is plotted with green lines in Fig. 3.

In the THz, it is possible to obtain τ_{tot} values in the 1–2-ps range, as is evident in Fig. 3(a), with a judicious engineering of the Hopfield coefficients. These values compare favorably with polariton-phonon scattering rates, even without adding the effect of final-state stimulation [28]. They also lie in the same range of the final-state stimulated scattering rates that are observed in exciton-polariton lasers [53]. We therefore suggest that polaritonic structures featuring dispersive MIM resonators might already constitute an interesting basis to develop a THz polariton laser.

The situation is different for devices operating in the mid-IR range of the spectrum. Based on the values reported in Table I, Fig. 3(b) shows that only τ_{tot} values well below 1 ps can be obtained. Polaritonic structures featuring MIM resonators are not a viable solution for mid-IR polariton lasers yet. However, the red curve in Fig. 3(b) shows that they are an excellent system to demonstrate the η_{QE} enhancement in the strong-coupling regime between light and matter, which has not been demonstrated to date. Furthermore, pump-probe experiments on the device architecture considered in this work are relatively straightforward [34], and they would allow one to validate the final-state stimulated scattering in ISB polaritonic systems, similarly to what was demonstrated for exciton polaritons 14 years ago in the seminal work by Savvidis *et al.* [7].

Finally, very little margin is available for near-IR ISB polariton devices at telecom wavelengths in the GaN/AlN system. The very short ISB transition lifetime (approximately 0.08 ps) restricts the device operation as LEDs as well as polariton lasers to a very narrow range of Hopfield coefficients. We believe, however, that they are worth development since the extremely high doping levels available in this system, in combination with a low dielectric constant for GaN and very thin QWs, can enable operation at the onset of the ultra-strong-coupling regime at telecom wavelengths. (A simple calculation shows that values of $\Omega_{Rabi}/\omega_{12} \approx 15\%$ should be attainable.) The observation of the peculiar phenomena arising from the ultra-strong-coupling regime —such as the generation of quantum vacuum radiation and of squeezed photons [54]—would be greatly simplified at $\lambda = 1.55\ \mu$m with respect to the THz and mid-IR, where proper detection technology is missing [55].

In the last part of the paper, we address the issue of designing a realistic optically pumped mid-IR polaritonic LED based on the MIM geometry and relying on phonon-polariton scattering (Fig. 2). To this scope, a simple rate-equation model is useful to estimate the external quantum efficiency of the system (η_{ext}), defined as P_{in}/P_{out}, where $P_{in,out}$ is the input-output power in W/cm^2. Based on the scheme of Fig. 2, we can write

$$\frac{dn_2}{dt} = \frac{AP_{in}}{\hbar\omega_{in}} - \frac{n_2}{\tau_{21}} - \frac{n_2}{\tau_{2NR}},$$
$$\frac{dn_1}{dt} = \frac{n_2}{\tau_{21}} - \frac{n_1}{\tau_{1tot}}, \quad (6)$$

where n_2 is the polariton density of the starting upper polariton state, n_1 is the polariton density of the $k = 0$ polariton state, ω_{in} is the frequency of the pump photon, $\omega_{out}$is the frequency of the emitted photon, τ_{21} is the

LO-phonon mediated scattering time between the UP (initial) and LP (final) states, τ_{2NR} is the UP lifetime stemming from all the other decay phenomena, τ_{1tot} is the total lifetime of the $k = 0$ LP state (radiative and nonradiative), and A is the absorption at the pump energy and angle. In the steady state, and recalling formula (2), we obtain

$$\eta_{ext} = \frac{P_{out}}{P_{in}} = \left(\frac{\omega_{out}}{\omega_{in}}\right)\left(\frac{\tau_{1tot}}{\tau_{1rad}}\right)\left(\frac{\tau_{2tot}}{\tau_{21}}\right)A = \eta_{freq}\eta_{QE}\eta_{pump}A. \quad (7)$$

This formula is a useful guide for device design. The absorption A does depend on α^2 approximately linearly. Caution is therefore needed: If α^2 is 0 or close to 0, absorption will be negligible. However, even with relatively moderate values of α^2, it is possible to increase the absorption by judiciously playing with the absolute radiative damping of the resonator. For instance, the technique described in Ref. [33] can lead—theoretically—up to critical coupling. An absorption >50% is, however, a good experimental start.

η_{freq} depends only on the input-output frequencies. This term is relatively favorable in the mid-IR, while in the THz it is necessarily smaller. At $f = 3$ THz, $\eta_{freq} = 0.25$, while at $f = 30$ THz, we obtain $\eta_{freq} = 0.7$.

η_{QE} is relatively under control, as shown in Fig. 3(b), and it is approximately 0.10/0.15.

Finally, η_{pump} can be tailored, since $1/\tau_{21}$, the phonon-polariton scattering rate, depends on the Hopfield coefficients as $(1-\alpha^2)$. It is crucial that the initial and final states contain a large matter fraction [28], since the polaritonic lifetimes in the mid-IR—as estimated in Fig. 3(b)—are in the sub-ps range. However, A also depends on α^2; hence, the quantity to maximize is A/τ_{12}, which is proportional to $\alpha^2(1-\alpha^2)$. The optimal choice—which maximizes A/τ_{12}—appears to be $\alpha^2 = 0.5$.

Based on these considerations, Fig. 5(a) reports the polaritonic dispersion $R(\omega, k)$ (reflectivity as a function of the in-plane wave vector) calculated with an rigorous coupled-wave analysis code [56] and the corresponding Hopfield coefficients for a mid-IR optically pumped polaritonic LED. It is a 1.1-μm-thick semiconductor slab containing 35 InGaAs/AlInAs QWs, sandwiched between two metallic surfaces. The QWs are 10 nm thick and doped to a sheet density of 1.3×10^{12} cm^{-2}. The top metallic surface is a 1D grating with period 3.25 μm and 80% filling factor. The calculations are performed with the same formalism of Ref. [34].

It appears that the best solution is to have even light-matter weights ($\alpha^2 = 0.5$) at $k = 0$. (Furthermore, given the microcavity dispersion, it is not possible to obtain a matter fraction larger than 50% for the LP at $k = 0$.) Figure 5(b) reports the corresponding Hopfield coefficients of the designed polaritonic system.

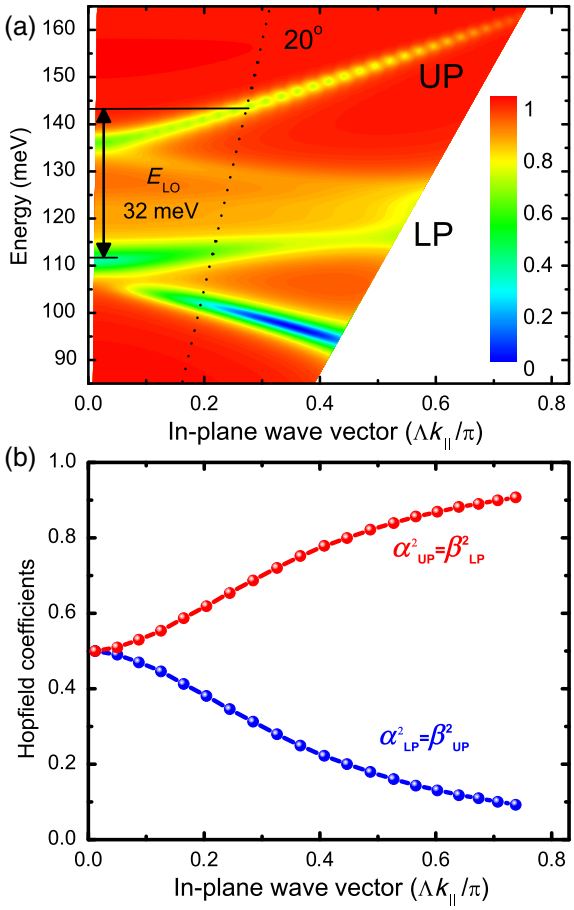

FIG. 5. (a) Optimal ISB polariton-dispersion diagram for an optical pumping experiment. The minimum Rabi splitting occurs at $k_{||} = 0$, and light is resonantly injected at an angle of 20°, one LO phonon away from the lower state minimum energy. The sample considered in this simulation consists of a repetition of 35 InGaAs/AlInAs QWs 10.5 nm wide separated by 15-nm-wide barriers. The sheet-doping density is 1.3×10^{12} cm^{-2}. The grating period is 3.25 μm, and its filling factor is 80%. (b) Hopfield coefficients of the polaritonic states as a function of the in-plane wave vector.

In the best-case scenario of a Rabi splitting of exactly one LO phonon, both initial and final states are located at $k = 0$. However, it is more practical to engineer the initial UP state at $k_{||}$ slightly different from 0, in order to simplify the experimental implementation. In the case of the proposed design, the sample must be pumped at an incident angle of 20 degrees at a wavelength $\lambda = 8.6$ μm. At this point, the initial UP polariton state exhibits a matter fraction of 30%. Polariton emission is expected to be orthogonal from the sample surface ($k_{||} = 0$) at a wavelength $\lambda = 11.48$ μm.

The design reported in Fig. 5 suits optical pumping experiments aimed at demonstrating enhanced ISB polariton emission at mid-IR frequencies. As a matter of fact, a quick estimate using formula (7) yields an external

quantum efficiency of the order of 1%, which would allow one to immediately verify the presence of enhanced emission. Furthermore, pump-probe experiments could be equally performed in order to validate if final-state stimulated scattering is indeed present. On the other hand, the very short total lifetimes, which are apparent from Fig. 3(b), suggest that mid-IR resonators with higher Q factors must be developed to demonstrate bosonic lasing.

In conclusion, we have discussed the opportunities arising from the development of ISB polariton lasers. It is our opinion that the potential of these devices has been underestimated, given, in particular, the possibility of operating them at high carrier densities without losing their bosonic character. This new degree of freedom implies operation at room temperature and relatively high output powers, not to mention the opportunities arising from a room-temperature Bose-Einstein condensate of charged bosonic excitations. We suggest a roadmap for the development of this new family of devices, consisting of three steps: (i) demonstration of the η_{QE} enhancement in mid-IR ISB polariton devices via optical pumping experiments, (ii) demonstration of final-state stimulated scattering in mid-IR ISB polariton devices via pump-probe experiments, and (iii) implementation of mid-IR dispersive resonators with high Q factors (at least a factor of 20 more with respect to current designs) to demonstrate optically pumped mid-IR polariton lasers. Finally, we stress that polaritonic structures featuring dispersive MIM resonators might already constitute a solid basis to develop a THz polariton laser.

We thank Daniele Bajoni and François Julien for useful discussions. We acknowledge partial support from the ERC "GEM" program (Grant Agreement No. 306661) and from the Triangle de la Physique (Project "INTENSE").

[1] C. Weisbuch, M. Nishioka, A. Ishikawa, and Y. Arakawa, *Observation of the Coupled Exciton-Photon Mode Splitting in a Semiconductor Quantum Microcavity*, Phys. Rev. Lett. **69**, 3314 (1992).

[2] D. Bajoni, *Polariton Lasers. Hybrid Light-Matter Lasers without Inversion*, J. Phys. D **45**, 313001 (2012).

[3] I. Carusotto and C. Ciuti, *Quantum Fluids of Light*, Rev. Mod. Phys. **85**, 299 (2013).

[4] A. Kavokin, J. J. Baumberg, G. Malpuech, and F. P. Laussy, *Microcavities* (Oxford University Press, New York, 2007).

[5] A. Imamoglu, R. J. Ram, S. Pau, and Y. Yamamoto, *Nonequilibrium Condensates and Lasers without Inversion: Exciton-Polariton Lasers*, Phys. Rev. A **53**, 4250 (1996).

[6] L. S. Dang, D. Heger, R. André, F. Bœuf, and R. Romestain, *Stimulation of Polariton Photoluminescence in Semiconductor Microcavity*, Phys. Rev. Lett. **81**, 3920 (1998).

[7] P. G. Savvidis, J. J. Baumberg, R. M. Stevenson, M. S. Skolnick, D. M. Whittaker, and J. S. Roberts, *Angle-Resonant Stimulated Polariton Amplifier*, Phys. Rev. Lett. **84**, 1547 (2000).

[8] F. Li, L. Orosz, O. Kamoun, S. Bouchoule, C. Brimont, P. Disseix, T. Guillet, X. Lafosse, M. Leroux, J. Leymarie, G. Malpuech, M. Mexis, M. Mihailovic, G. Patriarche, F. Réveret, D. Solnyshkov, and J. Zuniga-Perez, *Fabrication and Characterization of a Room-Temperature ZnO Polariton Laser*, Appl. Phys. Lett. **102**, 191118 (2013).

[9] P. Bhattacharya, T. Frost, S. Deshpande, M. Z. Baten, A. Hazari, and A. Das, *Room Temperature Electrically Injected Polariton Laser*, Phys. Rev. Lett. **112**, 236802 (2014).

[10] J. Zuniga-Perez, E. Mallet, R. Hahe, M. J. Rashid, S. Bouchoule, C. Brimont, P. Disseix, J. Y. Duboz, G. Gommé, T. Guillet, O. Jamadi X. Lafosse, M. Leroux, J. Leymarie, F. Li, F. Réveret, and F. Semond, *Patterned Silicon Substrates: A Common Platform for Room Temperature GaN and ZnO Polariton Lasers*, Appl. Phys. Lett. **104**, 241113 (2014).

[11] D. Dini, R. Köhler, A. Tredicucci, G. Biasiol, and L. Sorba, *Microcavity Polariton Splitting of Intersubband Transitions*, Phys. Rev. Lett. **90**, 116401 (2003).

[12] C. Sirtori, S. Barbieri, and R. Colombelli, *Wave Engineering with THz Quantum Cascade Lasers*, Nat. Photonics **7**, 691 (2013).

[13] R. Colombelli, C. Ciuti, Y. Chassagneux, and C. Sirtori, *Quantum Cascade Intersubband Polariton Light Emitters*, Semicond. Sci. Technol. **20**, 985 (2005).

[14] L. Sapienza, A. Vasanelli, R. Colombelli, C. Ciuti, Y. Chassagneux, C. Manquest, U. Gennser, and C. Sirtori, *Electrically Injected Cavity Polaritons*, Phys. Rev. Lett. **100**, 136806 (2008).

[15] S. I. Tsintzos, N. T. Pelekanos, G. Konstantinidis, Z. Hatzopoulos, and P. G. Savvidis, *A GaAs Polariton Light-Emitting Diode Operating near Room Temperature*, Nature (London) **453**, 372 (2008).

[16] D. Bajoni, E. Semenova, A. Lemaître, S. Bouchoule, E. Wertz, P. Senellart, and J. Bloch, *Polariton Light-Emitting Diode in a GaAs-Based Microcavity*, Phys. Rev. B **77**, 113303 (2008).

[17] A. A. Khalifa, A. P. D. Love, D. N. Krizhanovskii, M. S. Skolnick, and J. S. Roberts, *Electroluminescence Emission from Polariton States in GaAs-Based Semiconductor Microcavities*, Appl. Phys. Lett. **92**, 061107 (2008).

[18] L. Sapienza, A. Vasanelli, C. Ciuti, C. Manquest, C. Sirtori, R. Colombelli, and U. Gennser, *Photovoltaic Probe of Cavity Polaritons in a Quantum Cascade Structure*, Appl. Phys. Lett. **90**, 201101 (2007).

[19] M. Geiser, G. Scalari, F. Castellano, M. Beck, and J. Faist, *Room Temperature Terahertz Polariton Emitter*, Appl. Phys. Lett. **101**, 141118 (2012).

[20] P. Jouy, A. Vasanelli, Y. Todorov, L. Sapienza, R. Colombelli, U. Gennser, and C. Sirtori, *Intersubband Electroluminescent Devices Operating in the Strong-Coupling Regime*, Phys. Rev. B **82**, 045322 (2010).

[21] G. Gunter, A. A. Anappara, J. Hees, A. Sell, G. Biasiol, L. Sorba, S. De Liberato, C. Ciuti, A. Tredicucci, A. Leitenstorfer, and R. Huber, *Sub-cycle Switch-On of Ultrastrong Light-Matter Interaction*, Nature (London) **458**, 178 (2009).

[22] S. Zanotto, R. Degl'Innocenti, J.-H. Xu, L. Sorba, A. Tredicucci, and G. Biasiol, *Ultrafast Optical Bleaching of Intersubband Cavity Polaritons*, Phys. Rev. B **86**, 201302 (2012).

[23] G. Scalari, C. Maissen, D. Turcinkova, D. Hagenmuller, S. De Liberato, C. Ciuti, C. Reichl, D. Schuh, W. Wegscheider, M. Beck, and J. Faist, *Ultrastrong Coupling of the Cyclotron Transition of a 2D Electron Gas to a THz Metamaterial*, Science **335**, 1323 (2012).

[24] A. A. Anappara, S. De Liberato, A. Tredicucci, C. Ciuti, G. Biasiol, L. Sorba, and F. Beltram, *Signatures of the Ultrastrong Light-Matter Coupling Regime*, Phys. Rev. B **79**, 201303 (2009).

[25] D. Hagenmüller, S. De Liberato, and C. Ciuti, *Ultrastrong Coupling between a Cavity Resonator and the Cyclotron Transition of a Two-Dimensional Electron Gas in the Case of an Integer Filling Factor*, Phys. Rev. B **81**, 235303 (2010).

[26] Y. Todorov, A. M. Andrews, R. Colombelli, S. De Liberato, C. Ciuti, P. Klang, G. Strasser, and C. Sirtori, *Ultrastrong Light-Matter Coupling Regime with Polariton Dots*, Phys. Rev. Lett. **105**, 196402 (2010).

[27] S. De Liberato, C. Ciuti, and C. C. Phillips, *Terahertz Lasing from Intersubband Polariton-Polariton Scattering in Asymmetric Quantum Wells*, Phys. Rev. B **87**, 241304(R) (2013).

[28] S. De Liberato and C. Ciuti, *Stimulated Scattering and Lasing of Intersubband Cavity Polaritons*, Phys. Rev. Lett. **102**, 136403 (2009).

[29] L. Nguyen-thê, S. De Liberato, M. Bamba, and C. Ciuti, *Effective Polariton-Polariton Interactions of Cavity-Embedded Two-Dimensional Electron Gases*, Phys. Rev. B **87**, 235322 (2013).

[30] E. Rosencher and B. Vinter, *Optoelectronics* (Cambridge University Press, Cambridge, England, 2002).

[31] K. L. Campman, H. Schmidt, A. Imamoglu, and A. C. Gossard, *Interface Roughness and Alloy-Disorder Scattering Contributions to Intersubband Transition Linewidths*, Appl. Phys. Lett. **69**, 2554 (1996).

[32] A. Delteil, A. Vasanelli, P. Jouy, D. Barate, J. C. Moreno, R. Teissier, A. N. Baranov, and C. Sirtori, *Optical Phonon Scattering of Cavity Polaritons in an Electroluminescent Device*, Phys. Rev. B **83**, 081404 (2011).

[33] J. M. Manceau, S. Zanotto, I. Sagnes, G. Beaudoin, and R. Colombelli, *Optical Critical Coupling into Highly Confining Metal-Insulator-Metal Resonators*, Appl. Phys. Lett. **103**, 091110 (2013).

[34] J.-M. Manceau, S. Zanotto, T. Ongarello, L. Sorba, A. Tredicucci, G. Biasiol, and R. Colombelli, *Mid-infrared Intersubband Polaritons in Dispersive Metal-Insulator-Metal Resonators*, Appl. Phys. Lett. **105**, 081105 (2014).

[35] C. Gmachl, H. M. Ng, S.-N. George Chu, and A. Y. Cho, *Intersubband Absorption at* $\lambda \approx 1.55$ μm *in Well-and Modulation-Doped* GaN/AlGaN *Multiple Quantum Wells with Superlattice Barriers*, Appl. Phys. Lett. **77**, 3722 (2000).

[36] N. Iizuka, K. Kaneko, and N. Suzuki, *Near-Infrared Intersubband Absorption in* GaN/AlN *Quantum Wells Grown by Molecular Beam Epitaxy*, Appl. Phys. Lett. **81**, 1803 (2002).

[37] S. Sakr, P. Crozat, D. Gacemi, Y. Kotsar, A. Pesach, P. Quach, N. Isac, M. Tchernycheva, L. Vivien, G. Bahir, E. Monroy, and F. H. Julien, GaN/AlGaN *Waveguide Quantum Cascade Photodetectors at* $\lambda \approx 1.55$ μm *with Enhanced Responsivity and* ~40 GHz *Frequency Bandwidth*, Appl. Phys. Lett. **102**, 011135 (2013).

[38] M. Tchernycheva, L. Nevou, L. Doyennette, F. H. Julien, E. Warde, F. Guillot, E. Monroy, E. Bellet-Amalric, T. Remmele, and M. Albrecht, *Systematic Experimental and Theoretical Investigation of Intersubband Absorption in* GaN/AlN *Quantum Wells*, Phys. Rev. B **73**, 125347 (2006).

[39] N. Vico Triviño, G. Rossbach, U. Dharanipathy, J. Levrat, A. Castiglia, J.-F. Carlin, K. A. Atlasov, R. Butté, R. Houdré, and N. Grandjean, *High Quality Factor Two Dimensional GaN Photonic Crystal Cavity Membranes Grown on Silicon Substrate*, Appl. Phys. Lett. **100**, 071103 (2012).

[40] I. Roland, Y. Zeng, Z. Han, X. Checoury, C. Blin, M. El Kurdi, A. Ghrib, S. Sauvage, B. Gayral, C. Brimont, T. Guillet, F. Semond, and P. Boucaud, *Near-Infrared Gallium Nitride Two-Dimensional Photonic Crystal Platform on Silicon*, Appl. Phys. Lett. **105**, 011104 (2014).

[41] M. Cai, O. Painter, and K. J. Vahala, *Observation of Critical Coupling in a Fiber Taper to a Silica-Microsphere Whispering-Gallery Mode System*, Phys. Rev. Lett. **85**, 74 (2000).

[42] K. Vahala, *Optical Microcavities* (World Scientific, Singapore, 2004).

[43] J. J. Hopfield, *Theory of the Contribution of Excitons to the Complex Dielectric Constant of Crystals*, Phys. Rev. **112**, 1555 (1958).

[44] B. N. J. Persson and A. Baratoff, *Theory of Photon Emission in Electron Tunneling to Metallic Particles*, Phys. Rev. Lett. **68**, 3224 (1992).

[45] Y. Todorov and C. Sirtori, *Intersubband Polaritons in the Electrical Dipole Gauge*, Phys. Rev. B **85**, 045304 (2012).

[46] S. De Liberato and C. Ciuti, *Quantum Theory of Electron Tunneling into Intersubband Cavity Polariton States*, Phys. Rev. B **79**, 075317 (2009).

[47] S. De Liberato and C. Ciuti, *Quantum Model of Microcavity Intersubband Electroluminescent Devices*, Phys. Rev. B **77**, 155321 (2008).

[48] R. C. Miller, A. C. Gossard, D. A. Kleinman, and O. Munteanu, *Parabolic Quantum Wells with the* GaAs – $Al_xGa_{1-x}As$ *System*, Phys. Rev. B **29**, 3740 (1984).

[49] L. Brey, N. F. Johnson, and B. I. Halperin, *Optical and Magneto-optical Absorption in Parabolic Quantum Wells*, Phys. Rev. B **40**, 10647 (1989).

[50] M. Geiser, C. Walther, G. Scalari, M. Beck, M. Fischer, L. Nevou, and J. Faist, *Strong Light-Matter Coupling at Terahertz Frequencies at Room Temperature in Electronic LC Resonators*, Appl. Phys. Lett. **97**, 191107 (2010).

[51] W. Kohn, *Cyclotron Resonance and de Haas-van Alphen Oscillations of an Interacting Electron Gas*, Phys. Rev. **123**, 1242 (1961).

[52] P. Bhattacharya, B. Xiao, A. Das, S. Bhowmick, and J. Heo, *Solid State Electrically Injected Exciton-Polariton Laser*, Phys. Rev. Lett. **110**, 206403 (2013).

[53] H. Deng, H. Haug, and Y. Yamamoto, *Exciton-Polariton Bose-Einstein Condensation*, Rev. Mod. Phys. **82**, 1489 (2010).

[54] S. De Liberato, C. Ciuti, and I. Carusotto, *Quantum Vacuum Radiation Spectra from a Semiconductor Microcavity with a*

Time-Modulated Vacuum Rabi Frequency, Phys. Rev. Lett. **98**, 103602 (2007).

[55] T. Schwartz, J. A. Hutchison, J. Leonard, C. Genet, S. Haacke, and T. W. Ebbesen, *Polariton Dynamics under Strong Light-Molecule Coupling*, ChemPhysChem **14**, 125 (2013).

[56] S. Zanotto, R. Degl'Innocenti, L. Sorba, A. Tredicucci, and G. Biasiol, *Analysis of Line Shapes and Strong Coupling with Intersubband Transitions in One-Dimensional Metallodielectric Photonic Crystal Slabs*, Phys. Rev. B **85**, 035307 (2012).